Heat-Induced Dimerization of BCL-x_L through α-Helix Swapping†

Alexey Yu. Denisov,‡ Tara Sprules,§ James Fraser,‡ Guennadi Kozlov,‡ and Kalle Gehring*,‡,§

Department of Biochemistry, and Québec/Eastern Canada High Field NMR Facility, McGill University, Montreal, Québec H3G 1Y6, Canada

Received October 5, 2006; Revised Manuscript Received November 13, 2006

ABSTRACT: The dimerization of anti-apoptotic BCL-x_L by three-dimensional domain swapping has recently been discovered at alkaline pH; however, the high energetic barrier between the dimer and monomer forms of BCL-x_L prevents them from interconverting at room temperature and neutral pH. Here, we demonstrate that BCL-x_L dimers can be easily prepared by heating concentrated protein above 50 °C. The *38 kDa* BCL-x_L dimer was fully characterized by multi-resonance nuclear magnetic resonance (NMR) spectroscopy, and the mechanism of dimerization by α-helix swapping was confirmed. Dimerization strongly affects the NMR signals from the turn between helices α5 and α6 of BCL-x_L and a portion of the long loop between helices α1 and α2. Measurements of residual dipolar couplings demonstrate that the solution structure of the BCL-x_L dimer is very close to the crystal structure. Dimer formation does not prevent tight binding of ligands to the hydrophobic cleft of BCL-x_L; however, binding of a BID BH3−peptide or a polyphenol drug, gossypol, to BCL-x_L significantly slowed monomer−dimer interconversion and is an example of the control of BCL protein oligomerization by ligand binding.

Proteins of the BCL-2 family are key regulators of programmed cell death (apoptosis) (*1*, *2*). Members of the BCL-2 family contain four regions of sequence homology (BH1−BH4) and can be divided into three groups: anti-apoptotic proteins, pro-apoptotic multi-BH proteins, and BH3-only proteins. BCL-2 family proteins participate in homo- and heterodimerization in solution to inhibit or promote apoptosis (*3*−*6*), and interactions between BCL-2 family proteins are obviously important for understanding of the mechanism of apoptosis. Structures of such protein complexes have not been resolved in details, although structures of most individual proteins of the BCL-2 family have been solved (*7*). BH3-only proteins such as tBID or BIM could have dual functions: neutralization of pro-survival BCL-2 proteins and activation of pro-death BAX-like proteins (*4*). Pro-apoptotic BAK and BAX proteins oligomerize and form pores (channels) in the mitochondrial membrane through which cytochrome *c* and other proteins can escape (*8*−*10*), and determining the structure of these membrane pores remains a barrier toward fully understanding the process of apoptosis (*7*, *11*, *12*). Through the structures of the BAK and BAX oligomers, the molecular mechanism that controls mitochondrial outer membrane permeability could be elucidated. Possible models of BAK and BAX protein oligomerization have been discussed in the literature, including the involvement of the BH3 region, influence of the N or C tails, membrane-component participation, etc. (*5*, *13*−*17*). As well, complexes of BCL-2 family proteins on the membrane could require significant conformational rearrangement (*18*, *19*).

The BCL-x_L protein is the principal anti-apoptotic member of the BCL-2 family of proteins, and its canonical monomeric form has been studied extensively by nuclear magnetic resonance (NMR)[1] and X-ray methods (*20*−*23*). Structures of the BCL-x_L protein in complex with BH3−peptides from pro-apoptotic BAK, BAD, and BIM proteins have been investigated (*22*, *24*, *25*). Dramatic conformational changes were found for BCL-x_L interactions with phospholipid micelles (*26*, *27*). Also, homodimerization of BCL-x_L by sequestering its C-terminal membrane anchor was shown (*5*). Three-dimensional (3D) domain swapping is a relatively unusual phenomenon (*28*−*31*), and it was not known to occur in the BCL-2 family of proteins. BCL-x_L protein dimerization and oligomerization by 3D domain swapping in alkaline conditions was recently discovered (*32*). It was shown that the BCL-x_L dimer is constructed by swapping helices α6 and α7 between monomers. In the monomer, helices α5 and α6 lie approximately parallel to one another, joined by a turn, but in the dimer, helices α5 and α6 merge to form a long straight α helix. The hydrophobic clefts of both dimer halves remain available for BH3−peptide binding, and the dimers have increased pore-forming activity in comparison to monomeric BCL-x_L (*32*). In the present study, we show that BCL-x_L homo-dimerization via an identical α-helix swapping mechanism

† This work was supported by grants STPGP-269729-03 from the Natural Sciences and Engineering Research Council of Canada and MOP-82177 from the Canadian Institutes of Health Research. K.G. is a Chercheur National of the Fonds de la recherche en santé du Québec.

* To whom correspondence should be addressed: Department of Biochemistry, McGill University, 3655 Promenade Sir William Osler, Montreal, Québec H3G 1Y6, Canada. Telephone: (514) 398-7287. Fax: (514) 847-0220. E-mail: kalle.gehring@mcgill.ca.

‡ Department of Biochemistry.

§ Québec/Eastern Canada High Field NMR Facility.

[1] Abbreviations: DMSO, dimethylsulfoxide; DTT, dithiothreitol; EDTA, ethylenediaminetetraacetic acid; HPLC, high-pressure liquid chromatography; HSQC, heteronuclear single-quantum correlation; NMR, nuclear magnetic resonance; NOESY, nuclear Overhauser effect spectroscopy; ppm, parts per million; rmsd, root-mean-square deviation.

10.1021/bi062080a CCC: $37.00
Published on Web 12/29/2006

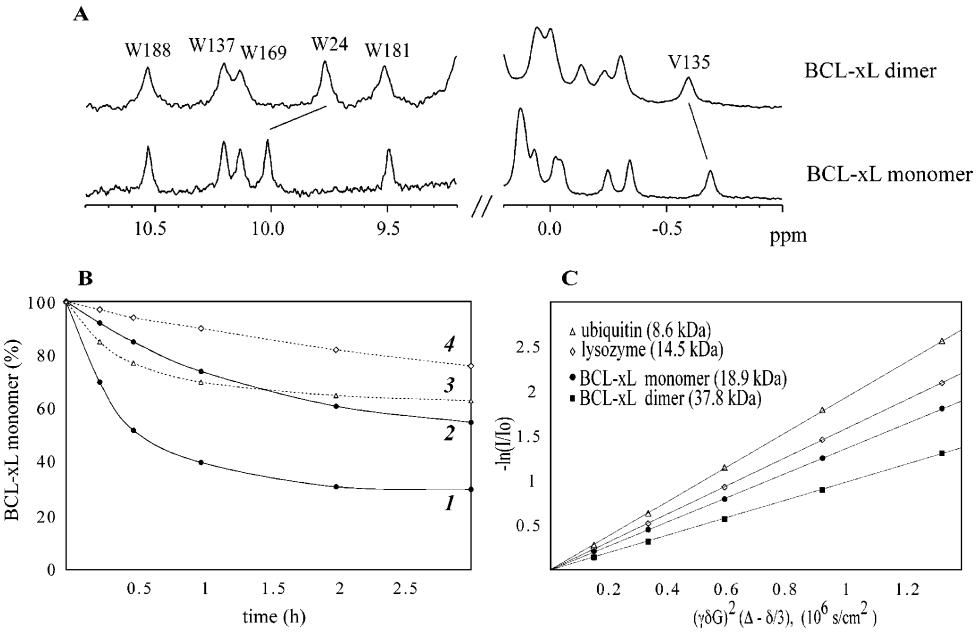

FIGURE 1: Identification of the BCL-x_L dimer. (A) Downfield (left) and upfield (right) proton NMR spectra of the five Trp HN-indole signals and the methyl group of Val-135 in the BCL-x_L dimer and monomer. (B) Kinetics of the monomer−dimer interconversion at 55 °C and neutral pH. Curves 1 and 2 present results at BCL-x_L concentrations of 1.0 and 0.35 mM; dashed curves 3 and 4 present results at a BCL-x_L concentration of 0.35 mM in the presence of either 10% DMSO or 10% DMSO plus 0.6 mM gossypol, respectively. (C) PFG NMR self-diffusion experiments of the BCL-x_L monomer and dimer forms and other proteins of known molecular weights (molecular weights in parentheses). The diffusion rate was measured from the slope of the log of the signal intensity (*I*) as a function of increasing gradient strength (*G*).

can be achieved by heating concentrated protein and present detailed NMR characterization of the dimer form. The recent demonstration that heat induces oligomerization of BAK and BAX proteins (*33*) suggests that 3D domain swapping could be a general feature of BCL-2 proteins.

EXPERIMENTAL PROCEDURES

Mouse BCL-x_L containing deletions in the C terminus (Δ197−233) and the internal loop (Δ45−84) was prepared as described earlier (*34*). For NMR studies, cultures were grown in M9 media supplemented with ^{15}N ammonium chloride and/or ^{13}C-enriched glucose to produce uniformly ^{15}N- or ^{15}N-,^{13}C-labeled proteins. Fractionally deuterated ^{15}N-,^{13}C-labeled BCL-x_L was prepared by growing cells in 80% D_2O. The monomer and dimer forms were purified by anion-exchange (Mono Q) high-pressure liquid chromatography (HPLC). The unlabeled 20 amino acid BH3−peptide from human BID (IIKNIARHLAQVGDSMDRSI) was chemically synthesized (BRI-NRC, Montreal, Canada). Gossypol was obtained from Sigma-Aldrich (St. Louis, MO) and used without further purification. NMR samples contained 0.2−1.5 mM protein in 90% H_2O/10% D_2O, 20 mM sodium phosphate (pH 7.0), 0.5 mM ethylenediaminetetraacetic acid (EDTA), and 3 mM dithiothreitol (DTT). NMR spectra were acquired at 30 °C on Bruker DRX 600 MHz and Varian Unity Inova 800 MHz spectrometers equipped with triple-resonance cryoprobes and pulsed-field gradients (PFGs). The following experiments were used for backbone and side-chain ^1H, ^{13}C, and ^{15}N resonance assignments: HNCACB, CBCA-(CO)HN, HNCA, HNCO, HN(CA)CO, and ^{15}N-edited nuclear Overhauser effect spectroscopy (NOESY) (*35*). For the BCL-x_L dimer, NMR spectra were recorded in the transverse relaxation-optimized spectroscopy (TROSY) mode (*36*). Amide heteronuclear $^{15}N\{^1H\}$-nuclear Overhauser effects (NOEs) were measured and used for determination of high-mobility regions of the protein (*37*). NMR spectra were processed using NMRPIPE (*38*) and XWINNMR (Bruker) software and analyzed with XEASY (*39*). The NMR signal assignments for the BCL-x_L dimer have been deposited in the BioMagnetic Resonance Bank (BMRB entry code 7013). PFG NMR self-diffusion experiments (*40*) for determination of diffusion coefficients were done with a PFG duration $\delta = 3.5$ ms and a time between PFG pulses $\Delta = 150$ ms. The gradient strength was calibrated by the PFG experiment for H_2O (*27*). $^{15}N-^1H$ residual dipolar couplings (RDCs) were extracted from semi-TROSY experiments with determination of the splitting along the proton axis (*41*) on an isotropic sample and on a sample containing 6 mg/mL Pf1 phage. MODULE software (*42*) was used for the comparison of the RDCs with their back-calculated values.

RESULTS AND DISCUSSION

Detection of BCL-x_L Dimers. The dimeric form of the BCL-x_L protein was first detected in NMR spectra (Figure 1A) and during protein purification by anion-exchange HPLC (Figure S1A in the Supporting Information) (*27*, *34*). Heating of the NMR sample increased the amount of the BCL-x_L dimer. The maximum temperature that did not cause strong BCL-x_L denaturation was determined to be 55 °C, and the kinetics of the interconversion were relatively fast at this temperature. At 1 mM protein concentration, approximately 70% of BCL-x_L was converted to the dimeric form in 2 h (Figure 1B). Gel-filtration chromatography (Figure S1B in the Supporting Information) and PFG self-diffusion NMR experiments (Figure 1C) demonstrated that this second form of BCL-x_L is a dimer. The ratio of diffusion coefficients for the dimer and monomer was close to 0.72, which is in good

agreement with the theoretical value for dimerization of a globular protein (*40*). Dimer formation was not sensitive to the salt concentration at neutral pH, and the monomer−dimer dissociation constant (K_d) was estimated to be 0.3 mM at 55 °C. Measurement of the rate of BCL-x_L dimer formation at different temperatures showed a strong temperature dependence. From an Arrhenius plot of ln(k) against (1/T), the interconversion barrier is estimated to be 80 kcal/mol at pH 7 (Figure S2A in the Supporting Information).

We investigated whether the BCL-x_L dimer obtained by heating is similar to the recently reported dimer that forms at pH 10 (*32*). The NMR spectra of the BCL-x_L dimers (Figures 1A and 2) induced by heating or alkaline pH were identical, confirming that our BCL-x_L dimer was also formed by α-helix swapping (*32*). We found that at 30 °C the BCL-x_L dimerization is 10^3 times faster at pH 10.0 than at pH 7.0, and at pH 10.0 and 1 mM protein concentration, the interconversion reaches equilibrium after around 10 h. We also studied the interconversion at 55 °C and four different pH values. These experiments showed a strong increase in the rate of dimer−monomer conversion at pH values higher than 8.0 (Figure S2B in the Supporting Information).

NMR Resonance Assignments of the BCL-x_L Dimer. We have carried out detailed NMR characterization of the BCL-x_L dimer. The extent of dimerization could be easily monitored by observing the position of the HN-indole signal of Trp-24 (Figure 1A). This residue is located in the long loop of BCL-x_L, close in space to the hinge/turn between helices α5 and α6, which undergoes a major conformational change during dimerization (*32*). Dimerization could also be monitored through the upfield methyl group of Val-135 (Figure 1A), which is more convenient in alkaline pH where the HN-indole signals are attenuated because of exchange with water. As was expected for the high-molecular-weight BCL-x_L dimer (38 kDa), signals of the amide protons in $^1H-^{15}N$ heteronuclear single-quantum correlation (HSQC) spectra of the fully protonated protein were broadened; therefore, a fractionally deuterated protein sample was used for the NMR assignments. The $^1H-^{15}N$ TROSY spectrum of the deuterated dimer showed good signal dispersion (Figure 2B), and 97% of the backbone amide resonances were identified and assigned by multidimensional NMR techniques.

Comparison of NMR Spectra. The regions of α-helical structure in the BCL-x_L dimer were determined on the basis of positive ^{13}C secondary chemical-shift values for α-carbon atoms (calculated as the observed minus random-coil chemical-shift values, $\Delta^{13}C^{\alpha}$) (*43*) and compared with the known structure of the monomer. The positions of the α helices are approximately the same in both the dimer and monomer (parts A and B of Figure 3). This is in full agreement with the crystal structure of the BCL-x_L dimer, which shows α-helical domain swapping (*32*). All $\Delta^{13}C^{\alpha}$ values were positive for the merged helices α5 and α6 in the BCL-x_L dimer, but they were negative for a few residues in the turn between helices α5 and α6 of the monomer. Similar results were obtained for the ^{13}C chemical shifts of carbonyl groups ($\Delta^{13}CO$) (data not shown). A detailed comparison showed the main difference [more than 1 part per million (ppm)] in the $\Delta^{13}C^{\alpha}$ values between the dimer and monomer in the hinge/turn between helices α5 and α6 (residues 157−163)

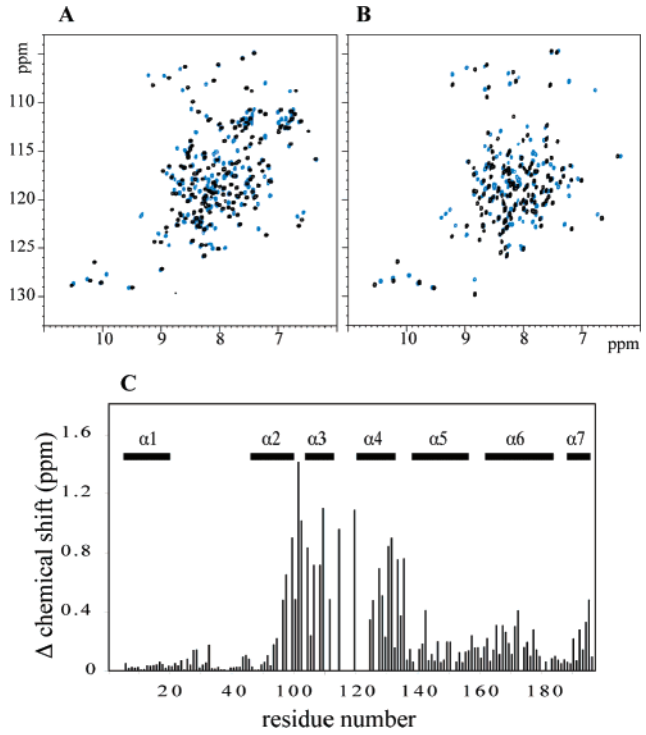

FIGURE 2: $^1H-^{15}N$ HSQC spectra and effect of BH3−peptide binding. (A) $^1H-^{15}N$ correlation spectra of the monomer and (B) fractionally deuterated dimer of BCL-x_L in the absence (black) and presence (blue) of bound BID BH3−peptide. (C) Magnitude of the amide chemical-shift changes $[(\Delta^1H \text{ shift})^2 + (\Delta^{15}N \text{ shift} \times 0.2)^2]^{1/2}$ in the BCL-x_L monomer upon BID BH3−peptide binding. The positions of α helices in BCL-x_L are shown.

and part of the long loop (residues 23−26), which is close in space to the turn between helices α5 and α6. The maximal differences were found for Lys-157 (3.6 ppm) and Met-159 (5.1 ppm), located in the turn between helices α5 and α6 in the monomer, which becomes α-helical in the BCL-x_L dimer. A comparison of $\Delta^{13}CO$ showed the largest effects for Lys-157 (4.4 ppm) and Glu-158 (3.6 ppm). Changes in the chemical shifts of amide HSQC signals also reveal the same regions affected upon dimerization (Figure 3C). The largest differences were observed for Ser-25 (1.4 ppm), Val-155 (1.1 ppm), and Gln-160 (1.3 ppm). These chemical-shift differences are mapped in red on the BCL-x_L dimer and monomer structures presented in Figure 4.

It is interesting that a perturbation of the initial (N-terminal) region of the long loop was observed in all NMR spectra, even though it does not participate directly in protein dimerization. To explain this result, we studied the heteronuclear $^{15}N\{^1H\}$-NOEs in both the dimer and monomer (Figure S3 in the Supporting Information). We found that the loop region, consisting of residues 20−27 (including the Trp-24 residue), has a rigid structure in the monomeric form with values of heteronuclear NOEs of 0.7−0.9. This is reflected in positive secondary chemical-shift values of $\Delta^{13}C^{\alpha}$ (Figure 3B) and an α-helical structure for residues 24−26 of the BCL-x_L monomer (see Figure 4). On the other hand, values of heteronuclear NOEs for residues 24−27 in the BCL-x_L dimer are in the range of 0.6−0.7, and Trp-24 is the last loop residue for which electron density was observed in the X-ray structure. This initial part of the long loop between helices α1 and α2 is more flexible in the dimer, which probably explains the difference in the chemical shifts.

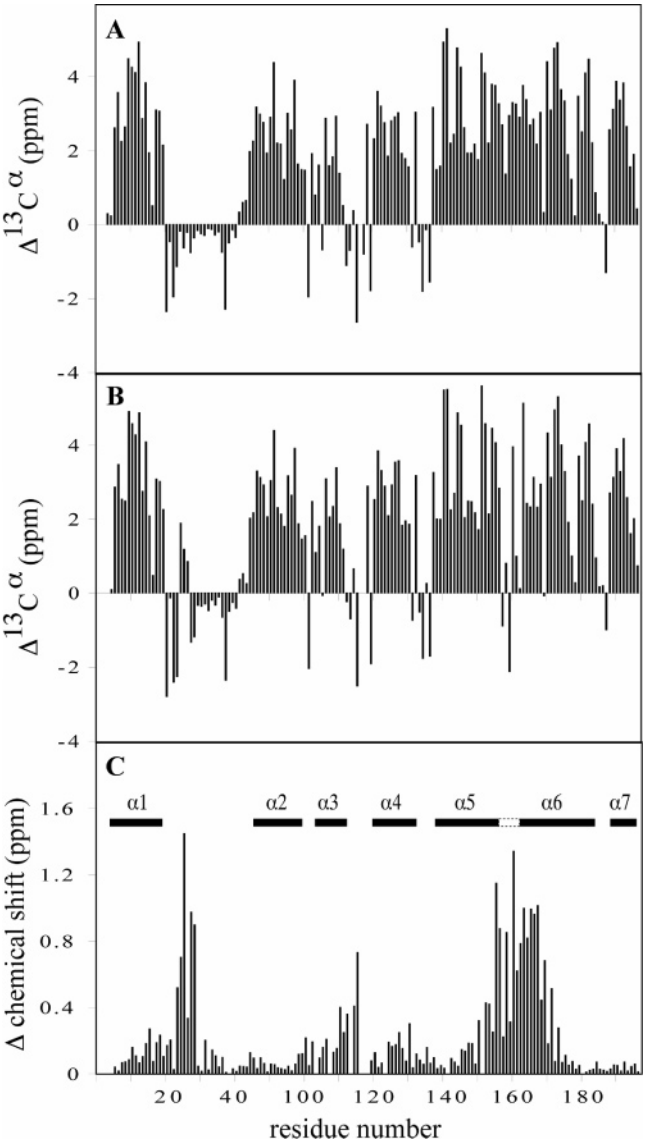

FIGURE 3: Comparison of NMR spectral parameters for the BCL-x_L dimer and monomer. Deviation of $^{13}C^{\alpha}$ chemical shifts from random-coil values for the dimer (A) and monomer (B) of BCL-x_L. (C) Magnitude of the amide chemical-shift changes in the $^{1}H-^{15}N$ HSQC spectra of the BCL-x_L dimer with respect to the monomer.

The remainder of the long loop (residues 28−82) is fully flexible in both the monomer and dimer of BCL-x_L.

Similarity of Solution and Crystal Structures of the Dimer. RDCs are widely utilized in structure determination to obtain the relative orientations of protein domains (*44*). A comparison of the crystal (*32*) and the solution structures of the BCL-x_L dimer was performed by a measurement of 117 $^{15}N-^{1}H$ RDCs in magnetically oriented Pf1 bacteriophages (Figure 5A). All RDCs for the merged helices α5 and α6 were positive. The experimentally measured RDCs fit well with back-calculated couplings based on the dimer crystal structure (Figure 5B). The *x* axis of the alignment frame coincided with the C_2-symmetry axis of the BCL-x_L dimer. RDCs for the flexible loop residues and two residues (Ser-110 and Leu-112) in the poorly resolved helix α3 in the crystal structure were excluded from the correlation. The same RDCs, when fit to the monomer structure, gave a root-mean-square deviation (rmsd) of 6.3 Hz between the calculated and observed couplings, with a large difference for the turn between helices α5 and α6 (for instance, $\Delta = 13.3$ Hz for Glu-158). This demonstrates that the measured RDCs are very sensitive to the structural changes between the monomer and dimer and that the conformation of the BCL-x_L dimer in solution is very similar to the crystal structure (*32*).

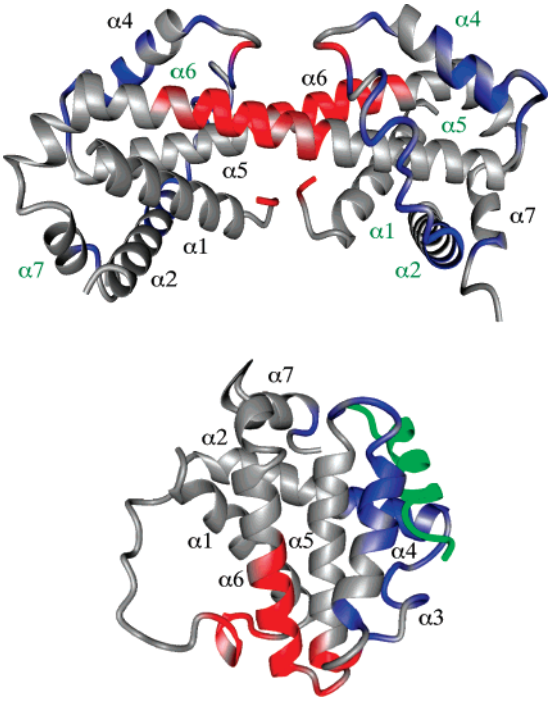

FIGURE 4: Mapping of BCL-x_L residues involved in dimerization and BH3−peptide binding. Ribbon representation of the crystal structure of the BCL-x_L dimer (top, PDB entry code 2B48) and the solution structure of the complex of the BCL-x_L monomer with the BAK BH3−peptide (bottom, PDB entry code 1BXL). Residues showing significant chemical-shift changes (>0.5 ppm in Figures 2C and 3C) upon dimerization and BID BH3−peptide binding are colored red and blue, respectively. The BAK BH3−peptide is shown in green.

BID BH3−Peptide and Small Inhibitor Binding. Tight binding of the BID BH3−peptide to the BCL-x_L dimer was detected by NMR with a complex stoichiometry of 2:1 peptide/dimer (Figure 2). This is in good agreement with the high-affinity binding ($K_d \sim 0.2$ μM) of a BAK BH3−peptide determined previously (*32*). A comparison of the HSQC spectra for the monomer and dimer in the absence and presence of the BID BH3−peptide (Figures 2) showed similar spectral changes upon BH3−peptide binding in the hydrophobic cleft of the protein. We were not able to assign the amide signals in $^{1}H-^{15}N$ HSQC spectra of the BCL-x_L dimer/BID BH3−peptide complex because of strong signal broadening at protein concentrations above 0.3 mM. On the other hand, around 90% of amide signals for the BID BH3−peptide complex with the BCL-x_L monomer could be assigned (Figure 2C). Significant chemical-shift changes were observed in regions of helices α2, α3, and α4, which belong to the hydrophobic cleft of the BCL-x_L protein. Similar changes were reported earlier for the BAD BH3−peptide/BCL-x_L monomer complex (*45*).

Mapping of BCL-x_L residues involved in the BID BH3−peptide complex formation (Figure 4) showed that dimerization and BH3−peptide binding take place at different sites on the BCL-x_L protein. Nevertheless, these two processes are not independent. Although the dimerization did not

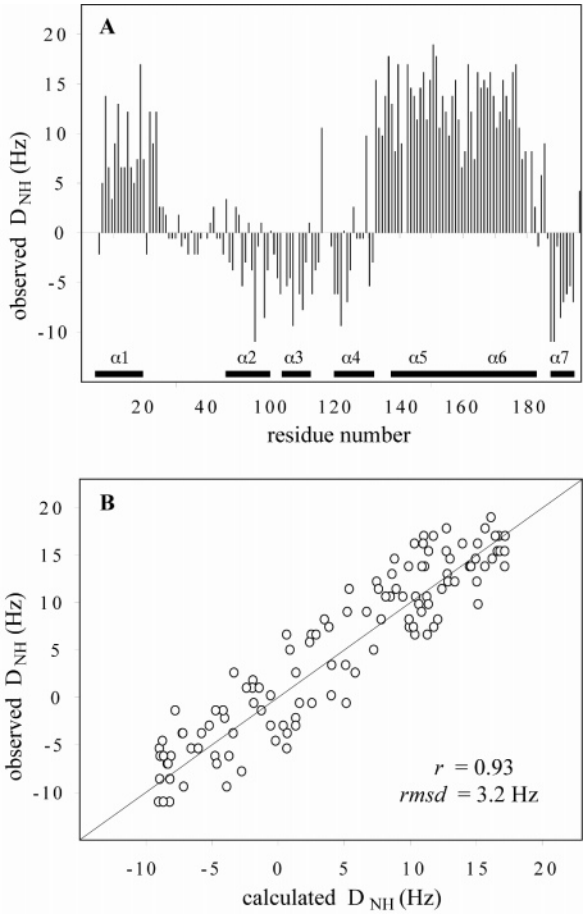

FIGURE 5: Values of RDCs in the BCL-x_L dimer measured in Pf1 phage (A) and the correlation between the observed RDCs and the calculated values for the crystal structure of BCL-x_L dimer (B). The axial (A_a) and rhombic (A_r) components of the alignment tensor are equal to 7.3×10^{-4} and 0.3×10^{-4}, respectively.

prevent tight BH3−peptide binding, peptide binding greatly slowed the interconversion process. After 1 day at 55 °C, no interconversion was detected for either BCL-x_L monomers or dimers in the presence of 1 mM BH3−peptide (at a 2:1 ratio of concentrations of the BID BH3−peptide to the BCL-x_L protein). Slow conversion of the BCL-x_L dimer−monomer was observed at the BH3−peptide concentration of 0.1 mM, probably because of the small amount of free protein in the solution (dissociated from the BH3−peptide). This finding can be explained if interconversion occurs by partial unfolding and loss of the BH3-binding site. Formation of stable BCL-x_L/BH3 peptide complexes would increase the energetic barrier of interconversion. Our results demonstrate that BH3−peptides provide a kinetic barrier to dimerization and oligomerization of BCL-x_L and explain the inhibition of BCL-x_L activity in membrane-pore formation (*32*).

We tested whether similar results could be obtained with "small molecule" inhibitors of BCL-x_L, which also bind the hydrophobic cleft of BCL-x_L (*7*, *12*, *46*). As an example, a polyphenol compound, gossypol, was used, which binds with a low micromolar dissociation constant (*47*). Because of the poor solubility of gossypol in water, the BCL-x_L interconversion experiments were performed in the buffer solutions with 10% dimethylsulfoxide (DMSO)-d_6. The addition of DMSO alone increased the initial rate of the monomer−dimer interconversion by 2−3 times, presumably by destabilizing the folded state (Figure 1B and Figure S2B in the Supporting Information). However, the subsequent addition of gossypol decreased the initial rate by 4−5 times, compared to the control DMSO solution. This demonstrates that binding of gossypol to BCL-x_L significantly blocks both the forward (Figure 1B) and backward (Figure S2B in the Supporting Information) reaction. The inhibition in the case of gossypol was weaker than for the BID BH3−peptide because of its weaker binding affinity to BCL-x_L and the smaller energetic stabilization of the complex.

CONCLUSION

The high energetic barrier between the protein monomer and domain-swapped dimer or oligomer can be modulated by the effects of heat, change of pH, mutations in the protein, binding of ligands, or the presence of detergents in the solution (*30*, *31*). Domain swapping induced by heat at neutral pH has been reported for bovine pancreatic ribonuclease (RNase A) (*48*) and cystatins (*49*). Here, we show that the temperature can also induce three-dimensional domain swapping in BCL-2 family proteins. The dimerization of members of the BCL-2 family by 3D domain swapping suggests that α-helix swapping could lead to the formation of higher oligomers (*32*). This is supported by the recent observation of BAX and BAK protein oligomerization and cytochrome *c* release from mitochondria induced by heating at 43 °C (*33*). The finding that BH3−peptide binding significantly slows α-helix swapping offers one explanation of how anti-apoptotic ligands prevent activation of the pro-apoptotic BCL proteins. While some ligands activate BAX and BAK (*50*, *51*), binding of anti-apoptotic BCL-2 family members should stabilize the folded state of BAX or BAK and raise the relative height of the energetic barrier to oligomerization as observed here for BCL-x_L dimerization.

SUPPORTING INFORMATION AVAILABLE

Separation of two forms of BCL-x_L by anion-exchange HPLC and gel-filtration chromatography, Arrhenius plot of the temperature dependence for the initial rate of the monomer−dimer conversion, the kinetics of the reverse dimer−monomer interconversion at different pH values and in the presence of DMSO and gossypol, and values of the $^{15}N\{^1H\}$ heteronuclear NOEs for backbone amides in the BCL-x_L dimer and monomer. This material is available free of charge via the Internet at http://pubs.acs.org.

REFERENCES

1. Danial, N. N., and Korsmeyer, S. J. (2004) Cell death: Critical control points, *Cell 116*, 205−219.
2. Cory, S., Huang, D. C. S., and Adams, J. M. (2003) The Bcl-2 family: Roles in cell survival and oncogenesis, *Oncogene 22*, 8590−8607.
3. Willis, S. N., Chen, L., Dewson, G., Wei, A., Naik, E., Fletcher, J. I., Adams, J. M., and Huang, D. C. S. (2005) Proapoptotic Bak is sequestered by Mcl-1 and Bcl-x_L, but not Bcl-2, until displaced by BH3-only proteins, *Genes Dev. 19*, 1294−1305.
4. Kuwana, T., Bouchier-Hayes, L., Chipuk, J. E., Bonzon, C., Sullivan, B. A., Green, D. R., and Newmeyer, D. D. (2005) BH3 domains of BH3-only proteins differentially regulate Bax-mediated mitochondrial membrane permeabilization both directly and indirectly, *Mol. Cell 17*, 525−535.

5. Jeong, S. Y., Gaume, B., Lee, Y. J., Hsu, Y. T., Ryu, S. W., Yoon, S. H., and Youle, R. J. (2004) Bcl-x_L sequesters its C-terminal membrane anchor in soluble, cytosolic homodimers, *EMBO J. 23*, 2146−2155.
6. Zhang, Z., Lapolla, S. M., Annis, M. G., Truscott, M., Roberts, G. J., Miao, Y., Shao, Y., Tan, C., Peng, J., Johnson, A. E., Zhang, X. C., Andrews, D. W., and Lin, J. (2004) Bcl-2 homodimerization involves two distinct binding surfaces, a topographic arrangement that provide an effective mechanism for Bcl-2 to capture activated Bax, *J. Biol. Chem. 279*, 43920−43928.
7. Petros, A. M., Olejniczak, E. T., and Fesik, S. W. (2004) Structural biology of the Bcl-2 family of proteins, *Biochim. Biophys. Acta 1644*, 83−94.
8. Kuwana, T., Mackey, M. R., Perkins, G., Ellisman, M. H., Latterich, M., Schneiter, R., Green, D. R., and Newmeyer, D. D. (2002) Bid, Bax, and lipids cooperate to form supramolecular openings in the outer mitochondrial membrane, *Cell 111*, 331−342.
9. Wei, M. C., Lindsten, T., Mootha, V. K., Weiler, S., Gross, A., Ashiya, M., Thompson, C. B., and Korsmeyer, S. J. (2000) tBID, a membrane-targeted death ligand, oligomerize BAK to release cytochrome *c*, *Genes Dev. 14*, 2060−2071.
10. Eskes, R., Desagher, S., Antonsson, B., and Martinou, J. C. (2000) Bid induces the oligomerization and insertion of Bax into the outher mitochondrial membrane, *Mol. Cell. Biol. 20*, 929−935.
11. Shi, Y. (2001) A structural view of mitochondria-mediated apoptosis, *Nat. Struct. Biol. 8*, 394−401.
12. Hinds, M. G., and Day, C. L. (2005) Regulation of apoptosis: Uncovering the binding determinants, *Curr. Opin. Struct. Biol. 15*, 690−699.
13. Tan, C., Drugosz, P. J., Peng, J., Zhang, Z., Lapolla, S. M., Plafker, S. M., Andrews, D. W., and Lin, J. (2006) Auto-activation of the apoptosis protein Bax increases mitochondrial membrane permeability and is inhibited by Bcl-2, *J. Biol. Chem. 281*, 14764−14775.
14. Reed, J. C. (2006) Proapoptotic multidomain Bcl-2/Bax-family proteins: Mechanism, physiological roles, and therapeutic opportunities, *Cell Death Differ. 13*, 1378−1386.
15. Ruffolo, S. C., and Shore, G. C. (2003) Bcl-2 selectively interact with the Bid-induced open conformer of Bak, inhibiting auto-oligomerization, *J. Biol. Chem. 278*, 25039−25045.
16. Terrones, O., Antonsson, B., Yamaguchi, H., Wang, H. G., Liu, J., Lee, R. M., Herrmann, A., and Basanez, G. (2004) Lipid pore formation by the concerted action of proapoptotic BAX and tBID, *J. Biol. Chem. 279*, 30081−30091.
17. Annis, M. G., Soucie, E. L., Dlugosz, P. J., Cruz-Aguado, A., Penn, L. Z., Leber, B., and Andrews, D. W. (2005) Bax forms multispanning monomers that oligomerize to permeabilize membranes during apoptosis, *EMBO J. 24*, 2096−2103.
18. Kim, P. K., Annis, M. G., Dlugosz, P. J., Leber, B., and Andrews, D. W. (2004) During apoptosis Bcl-2 changes membrane topology at both endoplasmic reticulum and mitochondria, *Mol. Cell 14*, 523−529.
19. Drugosz, P. J., Billen, L. P., Annis, M. G., Zhu, W., Zhang, Z., Lin, J., Leber, B., and Andrews, D. W. (2006) Bcl-2 changes conformation to inhibit Bax ologomerization, *EMBO J. 25*, 2287−2296.
20. Muchmore, S. W., Sattler, M., Liang, H., Meadows, R. P., Harlan, J. E., Yoon, H. S., Nettesheim, D., Chang, B. S., Thompson, C. B., Wong, S. L., Ng, S. C., and Fesik, S. W. (1996) X-ray and NMR structure of human Bcl-x_L, an inhibitor of programmed cell death, *Nature 381*, 335−341.
21. Aritomi, M., Kunishima, N., Inohara, N., Ishibashi, Y., Ohta, S., and Morikawa, K. (1997) Crystal structure of rat Bcl-x_L. Implications for the function of the Bcl-2 protein family, *J. Biol. Chem. 272*, 27886−27892.
22. Liu, X., Dai, S., Zhu, Y., Marrack, P., and Kapper, J. W. (2003) The structure of a Bcl-x_L/Bim fragment complex: Implications for Bim function, *Immunity 19*, 341−352.
23. Manion, M. K., O'Neill, J. W., Giedt, C. D., Kim, K. M., Zhang, K. Y., and Hockenbery, D. M. (2004) Bcl-x_L mutations suppress cellular sensitivity to antimycin A, *J. Biol. Chem. 279*, 2159−2165.
24. Sattler, M., Liang, H., Nettesheim, D., Meadows, R. P., Harlan, J. E., Eberstadt, M., Yoon, H. S., Shuker, S. B., Chang, B. S., Minn, A. J., Thompson, C. B., and Fesik, S. W. (1997) Structure of Bcl-x_L−Bak peptide complex: Recognition between regulators of apoptosis, *Science 275*, 983−986.
25. Petros, A. M., Nettesheim, D. G., Wang, Y., Olejniczak, E. T., Meadows, R. P., Mack, J., Swift, K., Matayoshi, E. D., Zhang, H., Thompson, C. B., and Fesik, S. W. (2000) Rationale for Bcl-x_L/Bad peptide complex formation from structure, mutagenesis, and biophysical studies, *Protein Sci. 9*, 2528−2534.
26. Losonczi, J. A., Olejniczak, E. T., Betz, S. F., Harlan, J. E., Mack, J., and Fesik, S. W. (2000) NMR studies of the anti-apoptotic protein Bcl-x_L in micelles, *Biochemistry 39*, 11024−11033.
27. Denisov, A. Y., Chen, G., Sprules, T., Moldoveanu, T., Beauparlant, P., and Gehring, K. (2006) Structural model of the BCL-w−BID peptide complex and its interactions with phospholipid micelles, *Biochemistry 45*, 2250−2256.
28. Bennett, M. J., Choe, S., and Eisenberg, D. (1994) Domain swapping: Entangling alliances between proteins, *Proc. Natl. Acad. Sci. U.S.A. 91*, 3127−3131.
29. Janowski, R., Kozak, M., Janowska, E., Grzonka, Z., Grubb, A., Abrahamson, M., and Jaskolski, M. (2001) Human cystatin C, an amyloidogenic protein, dimerizes through three-dimensional domain swapping, *Nat. Struct. Biol. 8*, 316−320.
30. Liu, Y., and Eisenberg, D. (2002) 3D domain swapping: As domains continue to swap, *Protein Sci. 11*, 1285−1299.
31. Bennett, M. J., Sawaya, M. R., and Eisenberg, D. (2006) Deposition diseases and 3D domain swapping, *Structure 14*, 811−824.
32. O'Neill, J. W., Manion, M. K., Maguire, B., and Hockenbery, D. M. (2006) BCL-x_L dimerization by three-dimensional domain swapping, *J. Mol. Biol. 356*, 367−381.
33. Pagliari, L. J., Kuwana, T., Bonzon, C., Newmeyer, D. D., Tu, S., Beere, H. M., and Green, D. R. (2005) The multidomain proapoptotic molecules Bax and Bak are directly activated by heat, *Proc. Natl. Acad. Sci. U.S.A. 102*, 17975−17980.
34. Denisov, A. Y., Madiraju, M. S. R., Chen, G., Khadir, A., Beauparlant, P., Attardo, G., Shore, G. C., and Gehring, K. (2003) Solution structure of human BCL-w: Modulation of ligand binding by the C-terminal helix, *J. Biol. Chem. 278*, 21124−21128.
35. Cavanagh, J., Fairbrother, W. J., Palmer, A. G., and Skelton, N. J. (1996) *Protein NMR Spectroscopy: Principles and Practice*, Academic Press, San Diego, CA.
36. Fernandez, C., and Wider, G. (2003) TROSY in NMR studies of the structure and function of large biological macromolecules, *Curr. Opin. Struct. Biol. 13*, 570−580.
37. Peng, J. W., and Wagner, G. (1994) Investigation of protein motions via relaxation measurements, *Methods Enzymol. 239*, 563−596.
38. Delaglio, F., Grzesiek, S., Vuister, G. W., Zhu, G., Pfeifer, J., and Bax, A. (1995) NMRpipe: A multidimensional spectral processing system based on UNIX pipes, *J. Biomol. NMR 6*, 277−293.
39. Bartels, C., Xia, T. H., Billeter, M., Güntert, P., and Wüthrich, K. (1995) The program XEASY for computer-supported NMR spectral analysis of biological macromolecules, *J. Biomol. NMR 5*, 1−10.
40. Altieri, A. S., Hinton, D. P., and Byrd, R. A. (1995) Association of biomolecular systems via pulsed field gradient NMR self-diffusion measurements, *J. Am. Chem. Soc. 117*, 7566−7567.
41. Lerche, M. H., Meissner, A., Poulsen, F. M., and Sorensen, O. W. (1999) Pulse sequences for measurement of one bond $^{15}N-^{1}H$ coupling constants in the protein backbone, *J. Magn. Reson. 140*, 259−263.
42. Dosset, P., Hus, J.-C., Marion, D., and Blackledge, M. (2001) A novel interactive tool for rigid-body modeling of multi-domain macromolecules using residual dipolar couplings, *J. Biomol. NMR 20*, 223−231.
43. Wishart, D. S., and Sykes, B. D. (1994) Chemical shifts as a tool for structure determination, *Methods Enzymol. 239*, 363−392.
44. Lipsitz, R. S., and Tjandra, N. (2004) Residual dipolar couplings in NMR structure analysis, *Annu. Rev. Biophys. Biomol. Struct. 33*, 387−413.
45. Petros, A. M., Fesik, S. W., and Olejniczak, E. T. (2005) ^{1}H, ^{13}C and ^{15}N resonance assignments of a Bcl-x_L/Bad peptide complex, *J. Biomol. NMR 32*, 260.
46. Reed, J. C., and Pellecchia, M. (2005) Apoptosis-based therapies for hematologic malignancies, *Blood 106*, 408−418.
47. Kitada, S., Leone, M., Sareth, S., Zhai, D., Reed, J. C., and Pellecchia, M. (2003) Discovery, characterization, and structure−

activity relationships studies of proapoptotic polyphenols targeting B-cell lymphocyte/leukemia-2 proteins, *J. Med. Chem. 46*, 4259−4264.

48. Park, C., and Raines, R. T. (2000) Dimer formation by a "monomeric" protein, *Protein Sci. 9*, 2026−2033.
49. Staniforth, R. A., Giannini, S., Higgins, L. D., Conroy, M. J., Hounslow, A. M., Jerala, R., Craven, C. J., and Waltho, J. P. (2001) Three-dimensional domain swapping in the folded and molten-globule states of cystatins, an amyloid-forming structural superfamily, *EMBO J. 20*, 4774−4781.
50. Walensky, L. D., Pitter, K., Morash, J., Oh, K. J., Barbuto, S., Fisher, J., Smith, E., Verdine, G. L., and Korsmeyer, S. J. (2006) A stapled BID BH3 helix directly binds and activates BAX, *Mol. Cell 24*, 199−210.
51. Moldoveanu, T., Liu, Q., Tocilj, A., Watson, M., Shore, G., and Gehring, K. (2006) The X-ray structure of a BAK homodimer reveals an inhibitory zinc binding site, *Mol. Cell 24*, 677−688.

BI062080A